Large-area Printed Supercapacitor Technology for Low-cost Domestic Green Energy Storage

Z. Tehrani [a]*, D.J. Thomas [a], T. Korochkina [a], C.O. Phillips [a], D. Lupo [b], S. Lehtima¨ki [b], J. O'Mahony [c] and D.T. Gethin [a]

[a] College of Engineering, Swansea University, Bay Campus , Swansea, SA2 8QQ, United Kingdom

[b] Department of Electronics and Communications Engineering, Tampere University of Technology, P.O.Box 692, 33710 Tampere, Finland

[c] Waterford Institute of Technology, Cork Road, Waterford City, Ireland

Abstract

In this research we demonstrate that a flexible ultra-thin supercapacitor can be fabricated using high volume screen printing process. This has enabled the sequential deposition of current collector, electrode, electrolyte materials and adhesive onto a Polyethylene terephthalate (PET) substrate in order to form flexible electrodes for reliable energy storage applications. The electrodes were based on an activated carbon ink and gel electrolyte each of which were formulated for this application. Supercapacitors that have surface areas from 100 to 1600mm^2 and an assembled device thickness of 375µm were demonstrated. The capacitance ranged from 50 to 400mF. Capacitance of printed carbon electrodes is rarely reported in literature and no references were found. The chemistry developed during this study displayed long-term cycling potential and demonstrated the stability of the capacitor for continued usage. The gel electrolyte developed within this work showed comparable performance to that of a liquid counterpart. This improvement resulted in the reduction in gel resistance from 90Ω to 0.5Ω. Significant reduction was observed for all resistances. The solid-state supercapacitors with the gel electrolyte showed comparable performance to the supercapacitors that used a liquid electrolyte. This large area printed device can be used in future houses for reliable green energy storage.

Keywords: Printed supercapacitor; green energy storage; activated carbon; gel electrolyte.

1. Introduction

Industrial green energy applications are reaching a point where their functionality is restricted by existing technologies for energy storage [1-4]. Conventional charge storage devices, including batteries, cannot provide the peak power needed for an energy intensive event without being heavy or unpractically large. Furthermore, there is a requirement for energy storage for emerging flexible and wearable electronics applications [5-8]for which a conforming, shaped footprint may be required. Also the move towards printable electronic components also necessitates a move towards printable energy storage. This would allow manufacture on similar production processes at corresponding speeds and with a complementary planar geometry.

Although, there have been reports of flexible energy storage [2-4] these have tended to be slimmed versions of conventional devices. Printable charge storage devices that can be easily fabricated using large-scale, solution-based processing, while still producing good electrochemical performance, are therefore required.
The supercapacitor history has more than a dozen years, but technique demand of such devices still makes scientists look for ways to reduce the cost of their development and production[9]. Recently the development of a low cost embedded system targeted to energy management in industrial environments has been started[10].
Also cost of product is very important by using printing techniques we are able to produce high volume with low cost product.

Supercapacitors, also known as electric double-layer capacitors or ultracapacitors [11], play a vital role in the technological evolution as their key attributes of high power density makes them preferred over batteries in a wide range of applications[12].

The performance of supercapacitors (SCs) lies between those of conventional electrolyte capacitors and rechargeable batteries. SCs have shorter charge and discharge durations than batteries and can manage a greater number of cycles, but with a lower overall capacity. Supercapacitors are also advantageous in terms of their environmental impact and safety [13, 14]. All-solid-state and flexible SCs are especially attractive energy storage devices for flexible and wearable applications [15, 16] because they have high power capacity, for example as a requirement for wireless communications and long cycle lifetime, requiring no maintenance or replacement [13, 14, 17].

Printed SCs require adequate electrochemical performance, as well as being mechanically robust and flexible [6, 18-20]. Carbon materials such as activated carbon and carbon nanotubes offer a number of characteristics making them well suited for active electrode materials, including high specific surface area, conductivity, high flexibility, regular pore structures, and electrochemical stability[21-23]. The electrolyte should ideally be made of flexible solid-state materials as liquid electrolytes are inherently prone to leakage and integrity problems [15, 24-29]. Presently, there are major hurdles in formulating a printable electrolyte that remains mobile and stable over the SC life. Currently, no printable solution has been formulated, and this prevents production of SCs on an industrial scale.

This work presents the development of an all printed layered supercapacitor in which high surface area carbon electrodes, electrolyte inks are formulated and then deposited by screen printing. As well as production of a functional printable electrolyte, which requires development of new formulations, there are a number of technical challenges in producing a successful all-printed supercapacitor. To prevent short circuits between the electrodes, a pinhole-free separator is vital and a durable seal against water vapour is necessary in order to avoid dehydration and breakdown of the SC. The objective of this research is to address these problems while demonstrating an approach that can be developed for mass manufacture on flexible

substrates, thus enabling these supercapacitors to become part of the next generation of power sources for renewable energy storage.

Fully printable flexible supercapacitors were therefore investigated and developed. Printable electrolyte and activated carbon materials were specifically developed for integrated manufacture in a stacked configuration by screen printing. The resulting supercapacitors were then characterised using electrical impedance spectroscopy. For comparison, a supercapacitor using a liquid electrolyte was also developed and tested.

2. Materials and methods

2.1 Supercapacitor Architecture

The SC architecture developed during this research is shown in **Figure 1**. This comprises a matched pairs of electrodes. These are composed of a flexible polymer substrate onto which a conductive silver layer is printed, to act as a current collector, and then overprinted with an activated carbon layer followed by a gel electrolyte. These are sandwiched together with an insulator/separator layer placed between.

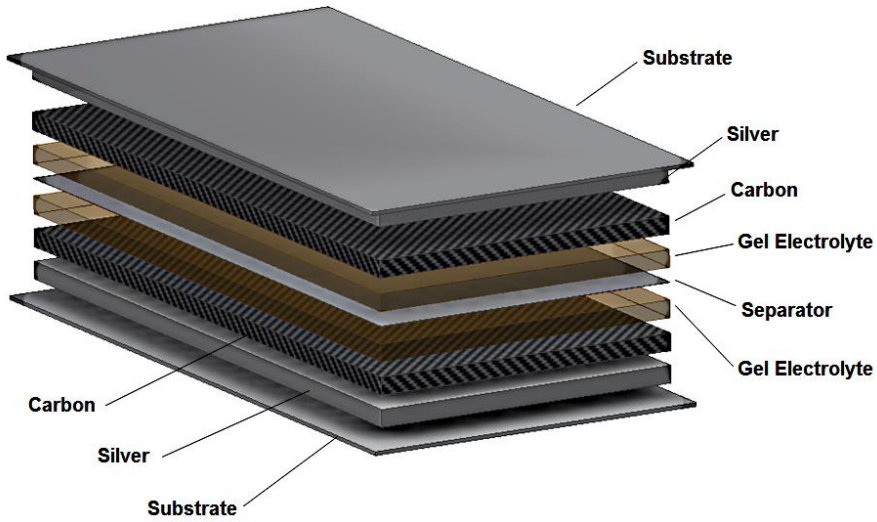

Figure 1. Schematic of the architecture of the all-printable supercapacitor

An adhesive band is also deposited on both electrodes to hold the assembled sandwich together. Using a gel electrolyte instead of an aqueous system is advantageous as it enables a printing route and simplifies encapsulation and through appropriate choice improves shelf life and the range of operating temperatures It is intended that the short, vertical ion path through a consistent thickness electrolyte and separator layer to the electrode layers leads to high charge and discharge currents with uniform performance across the electrodes.

2.2. Material fabrication

A PET substrate is favoured for use in printed electronics applications, including energy storage, due to its lower cost, high mechanical strength, flexibility, thermal stability and chemical resistance [6, 24, 30-33]. A transparent PET film ST506, 125 µm thickness was supplied by HiFi Industrial films. This film is heat stabilized to provide high temperature resistance and hence dimensional stability during processing.

Silver polymer ink (C2080415P2) was purchased from Gwent Electronic Materials (Pontypool, UK). This highly conductive silver polymer ink was selected for the printable current collector. It has been developed for a wide range of electronic applications and has the following characteristics necessary for this application: compatibility with activated carbon inks, high stability and long-term storage, excellent adhesion to PET substrates after sintering.

The carbon electrode layer was prepared from Norit DLC Super 50 activated carbon (Cabot Norit Nederland BV). This was mixed in-house with a polymeric binder and graphite to form a screen printable ink. Appropriate particle sizing and distribution of components in the ink was achieved via triple roll milling (Exakt 80E, EXACT Apparatebau GmbH & Co. KG, Germany).

The electrolyte comprised 0.21g Lithium Chloride (LiCl, Sigma Aldrich), 0.5g polyethylene oxide (PEO, Mv = 100,000, nd = 1.45, Sigma Aldrich) and 0.29g ethylene carbonate (EC Sigma Aldrich in 10mL tetra hydrofuran (THF, Sigma Aldrich The components were gradually added to the solvent during magnetic stirring in the order listed above. This composition was found to have insufficient viscosity for screen printing.

Extensive laboratory work based around a factorial approach on binder/solvent combinations established that the addition of 0.1% hydroxypropyl cellulose (Sigma Aldrich) increased the viscosity sufficiently to allow printing. A wet electrolyte, based on an aqueous lithium chloride was also trialed at the same concentration. A high electrolyte concentration was selected to ensure an excess of ions such that the risk for electrolyte starvation and additional internal resistance was removed [30].

To encapsulate the supercapacitors, a screen printable UV curable adhesive with an aliphatic urethane acrylate base was purchased (product name 3M Ltd). The separator was a TF4050 paper (Nippon Kodoshi Corporation).

2.3. Supercapacitor Fabrication

2.3.1 Screen printing

The supercapacitors were produced by first printing the silver current collector onto the PET substrate. On top of this was printed the activated carbon layer, with a 0.5 mm overlap to ensure the silver was fully covered with the carbon and did not contact the electrolyte (as it may interfere with electrochemical double layer formation due to possible involvement of silver ink in the redox reactions). A perimeter line of adhesive was printed, both to contain the electrolyte and hold the electrodes together, and the final printed layer was the electrolyte gel. The image

design and layout with respect to the printing direction (denoted by black arrow) are shown in **Figure 2**. The designs allowed supercapacitors from 100 to 1600 mm^2 to be produced. For the wet electrolyte supercapacitor, only silver and carbon layers were printed.

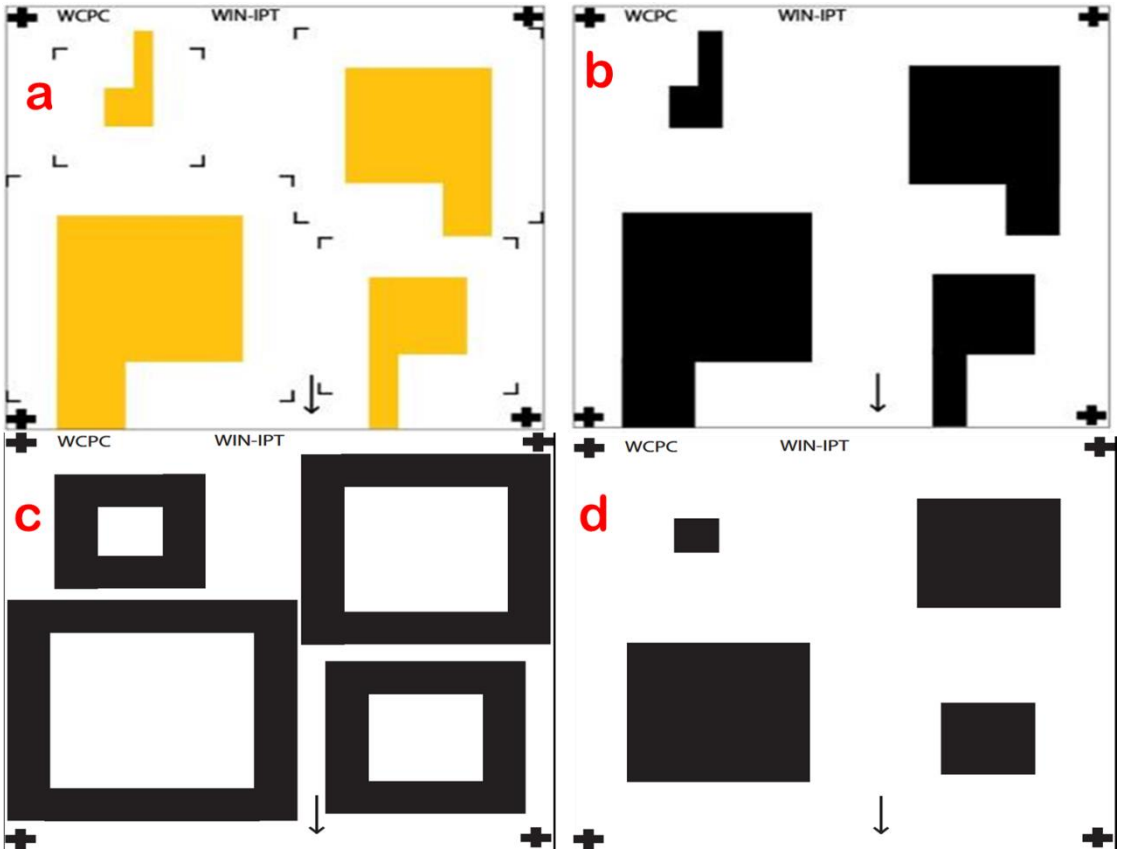

Figure 2. Solid area designs with respect to the printing direction (denoted by the black arrow) (a) for silver ink (Top left-yellow), (b) for activated carbon ink (right –top black), (c) for adhesive and (d) for electrolyte gel ink

Printing was carried out using a DEK 248 screen press. A range of screens were selected for each layer to give the appropriate layer thickness but machine settings were kept constant for all the layers (print flood speed 70 mm/s, 2 mm snap off, 10 kg squeegee load). To achieve the required thickness of carbon material, three layers were printed. The silver and carbon printed layers were first dried on a belt dryer and then placed in an oven to remove any residual solvents. The adhesive layer was cured using a UV dryer and the electrolyte was not dried. The screen selection and drying parameters are listed in Table 1. All layers were fully dried before the subsequent layer was printed.

Table 1. Summary of printing and drying settings

Ink	*Screen used*	*Drying regime*
Silver	*Polyester 77-55*	5 min at 130°C belt dryer, 5 min at 130°C in oven
Carbon	*Polyester 61-64*	5 min at 90°C belt dryer, 5 min at 100°C in oven
Adhesive	*Polyester 61-64*	UV cured two seconds at 600 mJ/cm^2
Gel electrolyte	*Polyester 61-64*	None

2.3.2 Assembly

For the fully printed supercapacitor, the separator was placed between the two electrodes and the whole assembly was then laminated together, using a laminating film, to form an air-tight seal. The SC's were then ready for testing. For the wet electrolyte supercapacitor, a double sided adhesive film (UPM Raflatac) was used as a barrier. A thin layer of electrolyte was applied via pipette onto one electrode, and a precut separator was applied to one of the two halves which were then brought together. Finally the whole assembly was encapsulated using adhesive tape. The total thickness of the assembly was below 400µm.

2.4 Characterisation

2.4.1 Printed layer topography

The deposited layers were characterised using scale-relevant techniques to ascertain both the thickness of the printed layers as well as the roughness and morphology of the surfaces. Three complimentary techniques were used, namely white light interferometry (WLI), scanning electron microscopy (SEM) and optical microscopy.

WLI (NT9300 optical profiling system (Veeco Instruments, Inc., Plainview, NY, USA) was used to measure the thickness of the overprinted silver and carbon layers as it was able to measure the surface of the transparent PET to provide a datum. WLI measurements were taken using 5 x magnifications, giving a measurement area of 1.3 mm by 0.9 mm with measurements taken over the printed edge.

For surface topography analysis of the printed carbon surface, measurements were taken using a 3D microscope (Alicona Infinite Focus G5 microscope (Alicona Imaging GmbH)) due to its ability to more effectively capture the surface form of carbon ink, which was resolved in less detail using white light interferometry due to the high level of light scattering. 3D microscope measurements were taken of the top surface of a single carbon layer printed directly on PET, three layers of carbon printed on PET and finally three carbon layers printed on a silver layer. Measurements were taken at both 10 and 100x magnification giving array sizes of 1.62 x 1.62 mm and 0.162 x 0.162 mm respectively. For all measured surfaces, five measurements were taken at each magnification. Topographical data was extracted

over the full 3D surface of each scanned area, after levelling along the measurement plane

Finally, SEM was used to view the morphology of the layers in cross section. Images were taken over the cross-section of the printed assembly by cutting the printed samples and positioning them to view the cut edge. In this measurement the focus was on viewing the layers rather than making dimensional measurements on the layers that comprise the electrode. The image was captured using a Hitachi S4800 SEM.

2.4.2 Performance testing of supercapacitors

The performance of the SC's and their component electrodes was evaluated using a potentiostat (Bio-logic Science Instruments' VMP3). Cyclic voltammetry (CV) measurement was performed with the potential scanned from 0 V to +0.7 V. The aim of this test was to see the shape of cyclic voltamogram and to confirm if it had a 'rectangular' shape that is characteristics of a capacitor and to calculate a preliminary capacitance value. Different sweep rates, 5, 10, 20, 30, 50 mV/s were used to find out which scan rate was most suitable for this measurement.

Capacitance and internal resistance was determined from galvanostatic discharge measurements. Understanding the charge transfer resistance at the electrode/electrolyte interface is key because this limits the performance of the supercapacitor. Linear Sweep Voltammetry (LSV), to establish the discharge characteristics, Constant Voltage (CsV), Constant current (CsI) tests were also performed. All tests were conducted in triplicate and in accordance with the International Standard ISC 62391-1:2006 [34].

First, the supercapacitor was charged from 0 to 0.7 V with a 1-min ramp, then held at 0.7 V for 30 min. After this charging time, the supercapacitor was discharged with a constant current. The capacitance was calculated from the voltage decline rate between 80 and 40 % of 0.7 V through $C = -I/(dV/dt)$. The leakage current of the supercapacitor at 0.7 V was obtained from the same measurement at the end of the charging phase [35]. The leakage current was defined at a reference temperature of 20 °C. A regulated power supply and a protective series resistance RS ≤ 1000 Ω was used. The error of measurement must be lower than ± 5 % (or 0.1 µA). Any variation in the leakage current is most likely due to variation in the electrode area and cross-sectional area of the gel electrolyte. Electrochemical Impedance Spectroscopy (EIS) was used to estimate the internal resistance and also the effects of charging and stability of supercapacitor performance.

3. Results and Discussion

3.1 Topography and morphology of supercapacitor construct

A sample surface topography plot that includes the edge of the silver layer overprinted with 3 layers of carbon is shown in **Figure 3**. The average height difference between the substrate and the top carbon surface was 62.7µm, with a standard deviation of 1.0 µm based on five measurements of an individual sample. On the print surface, regular topographical features were evident due to the

frequency and dimensions of the mesh used in screen printing. The highest points of the surface were indicated by an average R_z value of 79.8 µm (with standard deviation of 4.5 µm). Of this series of layers, the silver print constituted approximately 4µm of the overall thickness, with the remainder coming from the three layers of carbon.

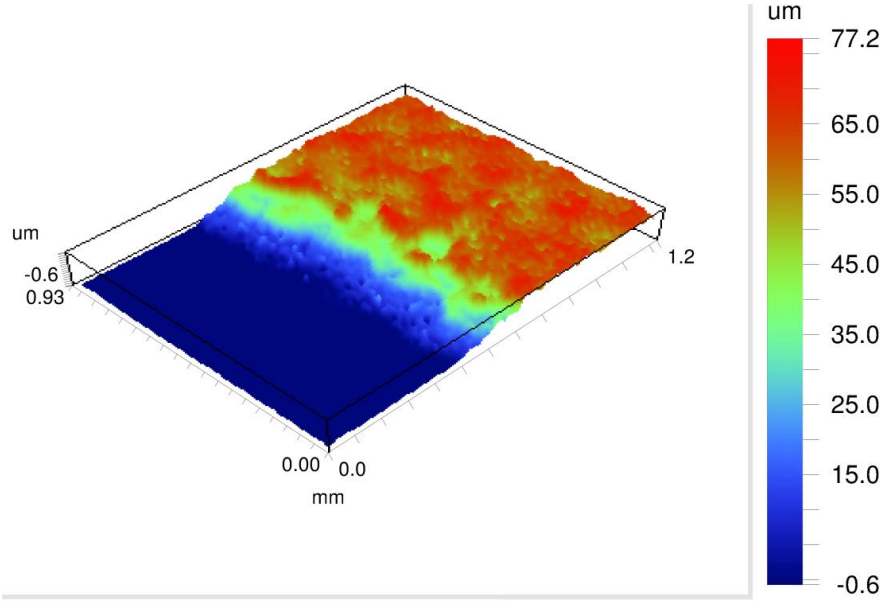

Figure 3. Surface topography over edge of print for silver layer overprinted with 3 layers of carbon-obtained using white light interferometry

Topographical data for the top surface of the three carbon layers printed on silver are shown in **Table 2** at both 10X and 100X magnification using 3D microscopy. Sample topography plots are also shown for both magnifications in Figure 4. When viewing the carbon surfaces at 10x magnification, undulations due to mesh marking are clearly evident. This was exacerbated by the stacking up of layers on top of one another which made the peaks and valleys in the surface more noticeable.

When viewing at 100x magnification, features due to the mesh were no longer evident and higher frequency roughness parameters due to the carbon particles dominated. In this case the roughness data influenced by larger features (S_z and $S10_z$) were more similar for single and triple layer prints while those due to high frequency roughness (S_a and S_q) were higher in the triple layer.

The true to projected surface area ratios (T/P) were calculated as 1.22, 1.27 and 1.30 for single layer carbon, triple layer carbon and triple layer carbon on silver respectively. This indicates that the roughness of the carbon surface, particularly for the triple layer, substantially increased the area available for activity when compared to a smooth planar surface.

Table 2. Surface roughness data for three carbon layers printed on silver using 3D microscopy.

Name	10 x magnification	100 x magnification	units	Description

Sa	1.575(0.066)	1.629(0.082)	µm	Average height of selected area
Sq	1.981(0.097)	2.043(0.076)	µm	Root-Mean-Square height of selected area
Sz	20.926(5.057)	24.968(4.813)	µm	Maximum height of selected area
S10z	17.429(2.487)	22.196(2.499)	µm	Ten-point height of selected area
T/P	1.030(0.001)	1.297(0.013)		True to projected surface area

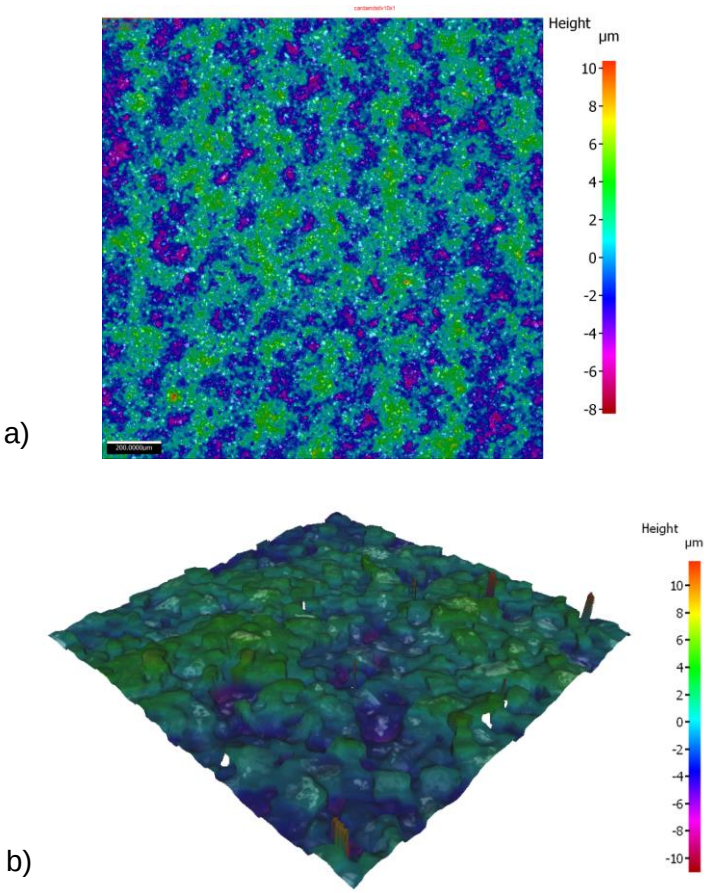

Figure 4. Sample surface topography plot of three carbon layers printed on silver obtained using 3D microscopy (a) 2D topography plot taken at 10x magnification indicating features due to screen printing mesh and (b) 3D topography plot taken at 100x magnification indicating features due to carbon particles

A sample SEM image of a cross-section of the construct is shown in Figure 5. The image highlights the rough, porous nature of the carbon layers. There were no visible interfaces between the carbon layers. The thickness of the triple carbon layer as suggested by analysis of the cross-section was similar to that measured using

white light interferometry but is subject to small discrepancy due to orientation of the sample and distortion induced by sample preparation.

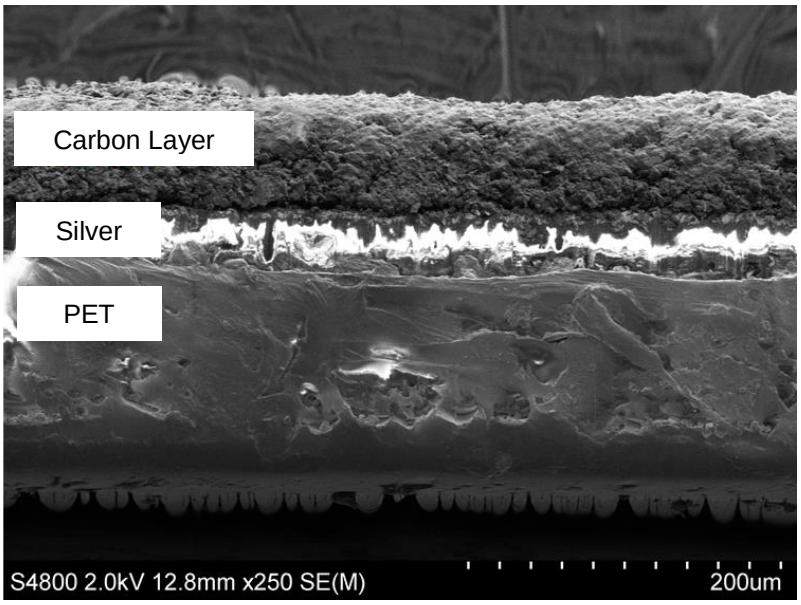

Figure 5. Morphology of cross-section of print for silver layer overprinted with three layers of carbon captured using SEM.

3.2 Performance of the Supercapacitors

Supercapacitors where manufactured and characterised according to the International Standard ISC 62391-1:2006 Class 3[34, 35]. In order to gain a detail understanding of the capacitor performance and the way in which the components influence this, a series of experiments were undertaken, notably CV, Linear Sweep Voltammetry (LSV), Constant Voltage (CsV), Constant current (CsI) as detailed in section 2.4.2. Understanding the charge transfer resistance at the electrode/electrolyte interface is key because this limits the performance of the supercapacitor.

Typical cyclic voltammograms from 0 V to 0.7 V of the gel supercapacitor at several sweep rates, 5, 10, 20, 30, 50 mV/s are shown in **Figure 6**. The results in **Figure 7** show the high electrical conductivity and the consistently good performance over a wide range of voltage scan rates.

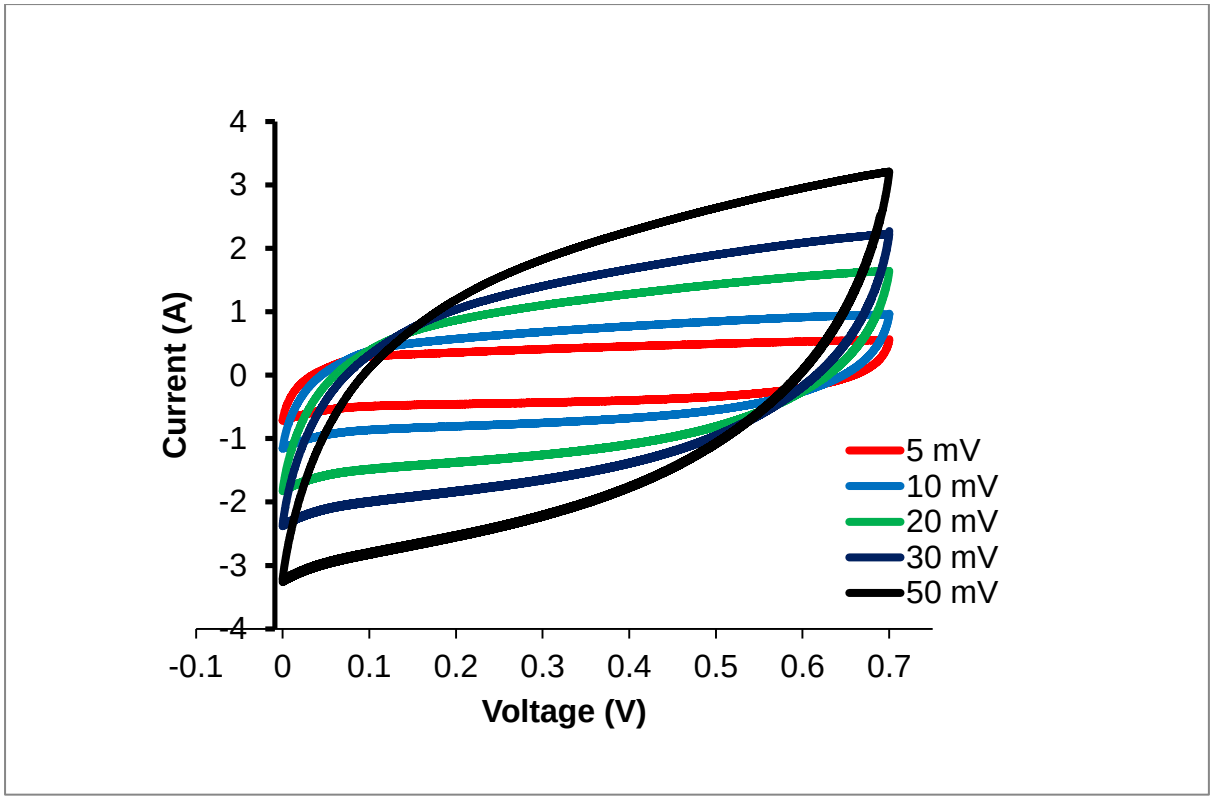

Figure 6. Cyclic voltamograms of the gel supercapacitor at different sweep rates of between 5-50mV.

The capacitance is shown in **Figure 7** and internal resistance as shown in **Figure 8** were determined from galvanostatic discharge measurements and are indicated in Table 3 for a number of tested supercapacitors. Capacitances for 400 and 600mm^2 sized supercapacitors were 166mF and 295mF respectively. These values may be compared with those reported in [35-37] where the devices were formed via casting and bar coating. The results also show a change in the capacitance with respect to area.

The reason for this is unclear, but it is most likely a result of dissimilar thicknesses of the gel and other small dimensional changes in the fabrication. This remains as a development to improve the consistency of these devices. As expected, the internal resistance was larger for the smaller supercapacitor, at 31Ω, whereas for the larger one it was 26Ω.

The larger internal resistance can be explained as both a resistance in the current collector contact pads, which were narrower in the smaller supercapacitor, as well as a smaller cross-sectional area of the electrolyte, which inhibits the movement of current-carrying ions.

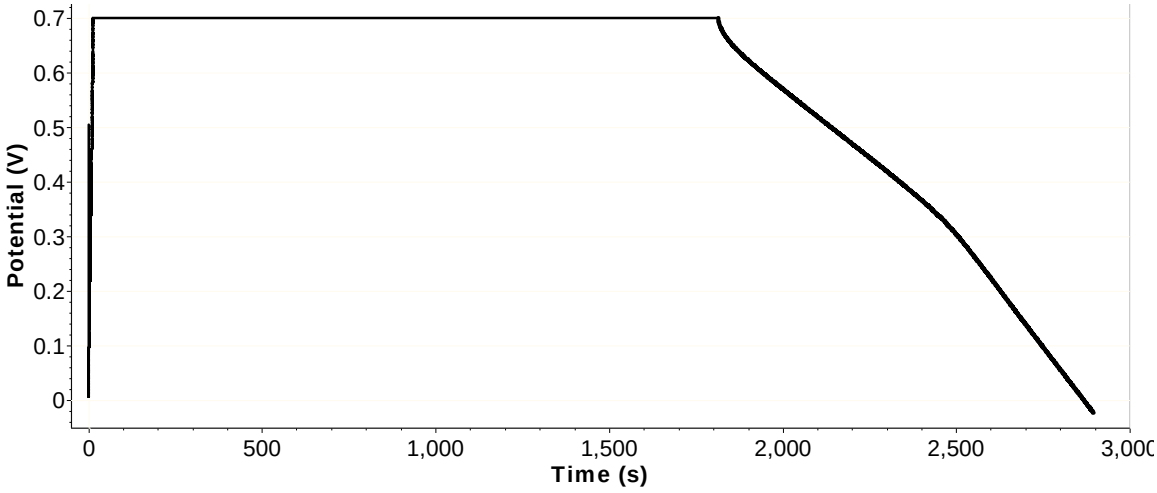

Figure 7. Typical galvanostatic discharge curve of the gel supercapacitor at constant discharge current for capacitance determination.

The internal resistances were calculated using equation below:

$$R = \Delta U_R / I$$

Where the voltage drop (ΔU_R =IR) was determined as the point of intersection between the linearly extrapolated voltage curve and the time axis immediately after starting the discharge of supercapacitor as shown in **Figure 8**.

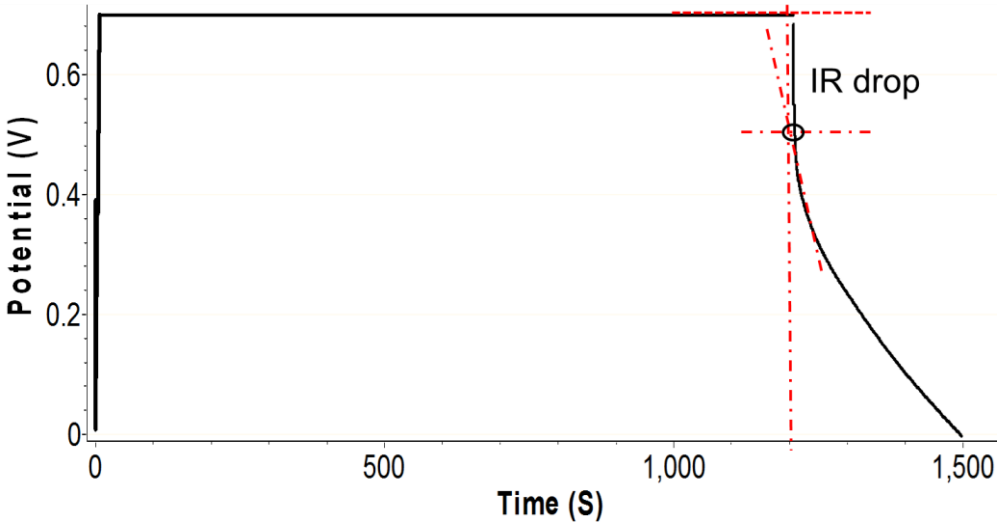

Figure 8. Galvanostatic discharge curve of the gel supercapacitor at constant discharge current for internal resistance determination.

Table 3. Supercapcitor characteristics obtained from galvanostatic measurements (ISC 62391-1:2006, Class 3).

Sample	Electrolyte	Electrode area cm^2	Capacitance, mF	C/A, mF/cm^2	IR, Ω	Leakage current, μA
S1	Liquid (LiCl in water)	9	450	50	-	95
S2	Gel	4	166	41	31	51
S3	Gel	6	295	49	26	34
S4	Gel (homogenized)	4	320	80	-	31

Four different supercapacitors were fabricated. S1 used a water based electrolyte as a reference whereas S2, S3 and S4 used a gel electrolyte, with gel preparation in S4 employing a homogenizer to maximize uniformity of blending. Noting that leakage current flows when the supercapacitor is fully charged and the voltage across the supercapacitor reaches the applied voltage E. The leakage current of three supercapacitors samples (S1, S2 and S3) was found to be 95 μA, 51 μA, and 34 μA respectively. The difference between S2 and S3 is only difference at the area.

In **Table 3** by comparing samples S1 and S2 in terms of capacitance per unit area with different electrolyte the water based system exhibits a higher specific capacitance coupled with a higher leakage current. In comparing S1 with S3, the capacitance is very comparable and the leakage current for S3 is significantly lower.

By comparing samples S2 withS3 and S4 there are very significant performance improvements. The gel used in S4 was prepared using a homogenizer; this improved the uniformity of the gel and also the uniformity of the coatings. This improved electrical conductivity which was reported in the **Table 3** which the uniformity of the gel has a significant effect on the capacitance of the SC. These results lead to the conclusive recommendation the gel should wet the electrode completely.

3.3. Electrochemical Impedance Spectroscopy

Electrochemical Impedance Spectroscopy (EIS) was also used to characterize the electrical performance of the supercapacitors. Several EIS measurements were performed and three components of the measurement were identified as: charge transfer through the activated carbon to the silver, charge transfer resistance of the gel and cross cell diffusion. It has been shown that solvent type has an effect on the performance of the electrolyte. Replacing some water with Tetrahydrofuran (THF) in the gel electrolyte reduced gel resistance most likely due to improved ionic mobility and wettability the formulation for prepare the gel was described at section 2.2.

In order to analyse the charge transfer and diffusion characteristics, some supercapacitors were manufactured with the water based printable gel electrolyte which was screen printed over electrodes.

The supercapacitor shows one large loop at high frequency, which is hypothesised to be the charge transfer resistance followed by several indistinct effects at medium frequencies followed by the sloped region. The sloped region may be linked to the electrolyte penetration into electrode poress as described by the equation 1.The impedance of the porous electrode is described by the following equation [38]:

$$Z_P = \sqrt{R_P Z_E}\,\mathrm{cotanh}\left(\sqrt{R_P/Z_E}\right)(\Omega) \quad (1)$$

$$Z_{SC} = R_S + ZE\,(\Omega) \quad (2)$$

Where Z_P is the impedance due to the porosity of the electrode; R_P is the ionic resistance of the active material; and Z_E is the electrode/electrolyte interface impedance, which is the voltage propagation through the porous electrode. The knee frequency delimiting the sloppy region and the vertical one as shown in **Figure 9** is not reached. This indicates that the ions do not cover the whole electrode surface when the capacitance is no longer frequency dependent (vertical region). This is most likely due to closed/narrow pores when the whole electrode surface is not accessible to ions.

The large loop at high frequency is indicative of the pseudocapacitive electrode [30]. The de Levie model which is a theory for a porous electrode, the impedance can be expressed in function of the cylindrical pore characteristics such as the pore length, the pore radius and the number of pores [32, 39] could not be used in this case as more complex dispersions need to be taken into account such as distribution of active sites, shape of the pores, electrode roughness, etc. Therefore, these curves were not modelled due to the difficulties in resolving individual features within the spectra. Both the diffusion and charge transfer impedances reduce with increased time. By examining how the curve changes after 48 hours it can be concluded that both the diffusion and charge transfer improve during this time.

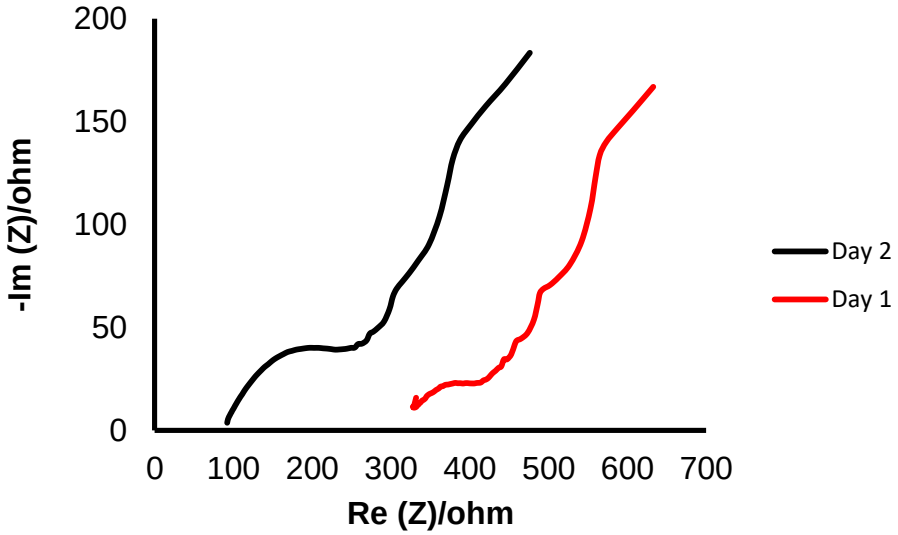

Figure 9. Impedance characteristics of supercapacitor at different days black curve – after 2 days of fabrication, red curve – after 1st day of fabrication without a vacuum seal.

Figure 9 compares the electro impedance spectra for the supercapacitor from this type with the gel electrolyte measured on day 1 with that measured on day 2. These curves were not modeled due to the difficulties in resolving individual features within the spectra. In order to be able to extract accurate charge transfer data it is preferable to use an equivalent circuit model, although, resistances can be directly read from the x- axis if a model is not available.

The day 2 spectra showed more than threefold reduction in gel and charge transfer resistance in the high frequency part of the spectra. This is most likely due to improved charge transfer kinetics after complete wetting of the porous electrodes was achieved. The gel electrolyte resistance decreased from about 320Ω to about 90Ω. This is in good correlation with the results obtained by transient techniques such as cyclic voltammetry and galvanostatic cycling according to international standards ISC 62391-1:2006. The resistance at the same frequency of 44.5Hz decreased from about 417Ω to about 219Ω, **Figure 10.** Further tests are needed to understand the cause of this difference.

The supercapacitor assembled in ambient conditions all impedances have not changed over time. Furthermore, there is a dramatic decrease in all resistances. There is about 180 times decrease in gel electrolyte resistance. This is most likely due to improved ion mobility as well as wettability of the electrode surface. There is also a significant reduction of an order of magnitude in charge transfer and diffusion resistance. This might be due to improved ion mobility as well as reduced amount of oxygen. But further tests are needed to understand the cause of these improvements.

Figure 10 shows the Nyquist plot from impedance testing of capacitor between 10 kHz and 1 Hz; each carbon electrode has an area of 200 mm^2 and mass

of 40mg. The supercapacitor demonstrates only a 0.4 Ω internal resistance for the gel electrolyte

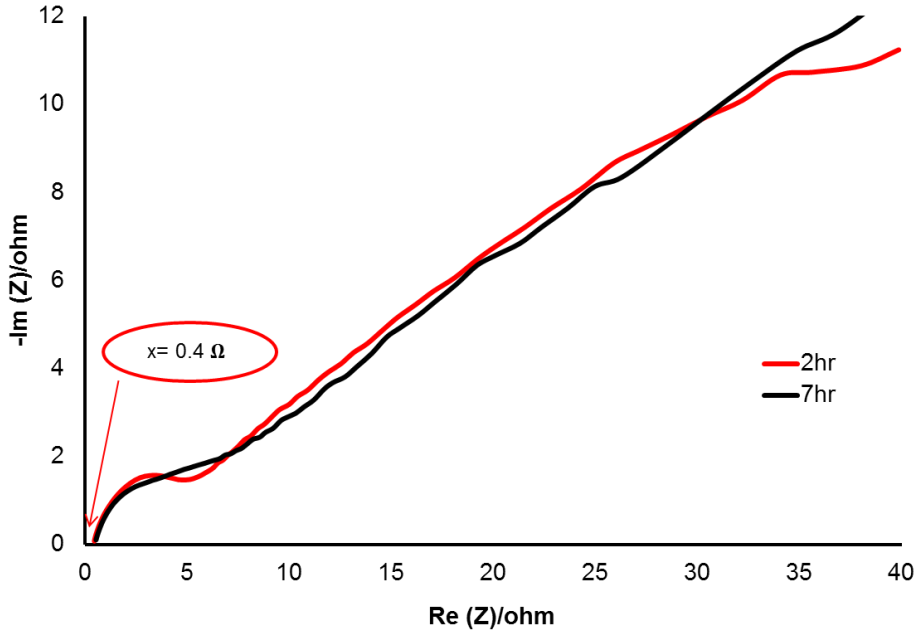

Figure 10. Impedance characteristics of gel electrolyte supercapacitor at different times: top graph - Nyquist plot, bottom graph - phase angle plot; red curve – 2 hours after fabrication, black curve – 7 hours after fabrication.

The effect of oxygen on active sites is not fully understood by the academic community. It is still the area of debate whether different quantities of oxygen are responsible for a change in a supercapacitor performance. This is an area which area, which requires more investigation, specifically examining the surface chemistry of activated carbon materials.

As shown on **Figure 9** the internal resistant (90Ω) is higher than **Figure 10** (0.4Ω). Significant improvements were achieved in printed supercapacitor performance in terms of internal resistance. There are several areas such as optimisation of electrode porosity, further optimisation of electrolyte formulation and improvement to encapsulation of electrodes needs to be looked into. These are some of the areas which require further investigation [35-37].

4. Conclusions

The following conclusions can be drawn from this work:

- It has been successfully demonstrated that all printable and flexible supercapacitors based on activated carbon and gel electrolyte have great potential as printed charge storage devices.
- The device performance spans the typical range of conventional supercapacitors used in large area energy storage applications
- The simplified architecture with the use of printable materials has the potential to lead to a new class of printable, cheap, flexible, and light charge storage

devices allowing for full integration with the emerging field of printed electronics.

- The silver/activated carbon- and gel-based supercapacitors may hold great potential for low-cost and high-performance flexible energy storage applications.
- All printed supercapacitors have a number of advantages: due to multi-layer design they can be manufactured by printing at low cost. The specific capacitance of the supercapacitor was 21 F/g, when only the total activated carbon mass in the device was taken into account. This value is of similar magnitude to previous results with printed activated carbon supercapacitors.
- A possible reason for the difference is the compression of the activated carbon electrode, which improves the contact between the carbon particles.
- The particles in the printed, non-compressed layers may not be fully in contact with each other or the current collector, reducing the effective amount of active electrode material.

5. Acknowledgments:

The authors wish to acknowledge The European Regional Development Fund (ERDF) through the Ireland Wales Program INTERREG 4A, for financial funding of this project also Prof. Marta Gunde, Dr Jože Moškon from National Institute of Chemistry, Ljubljana, Slovenia.

6. Nomenclature

CV	Cyclic Voltammetry
CsI	Constant current
CsV	Constant Voltage
EC	Ethylene carbonate
EIS	Electrochemical Impedance Spectroscopy
GCPL	Galvanostatic Cycling with Potential Limitation
Gem	Gwent Electronic Group
IR	internal resistance
IPA	Isopropyl alcohol
OCV	Open Circuit Voltage
LiCl	Lithium Chloride
LSV	Linear Sweep Voltammetry
PEO	Poly ethylene oxide
PET	Polyethylene terephthalate
R2R	Roll-to-Roll
SCs	Supercapacitors
SEM	Scanning Electron Microscope
THF	Tetra hydrofuran
UV	Ultra violet

WLI White light interferometry

References

1. He, X. *Flexible, Printed and Thin Film Batteries 2015-2025: Technologies, Forecasts, Players*. 2016; Available from: http://www.idtechex.com/research/reports/flexible-printed-and-thin-film-batteries-2015-2025-technologies-forecasts-players-000410.asp.
2. PowerStream. *Ultrathin Rechargeable Lithium Polymer Batteries from PowerStream*. 2016 Available from: www.powerstream.com/thin-lithium-ion.
3. Ltd, C.-X.P. *Supercapacitors Product Guide 2014 - Cap-XX*. 2014; Available from: www.cap-xx.com/wp-content/.../04/CAP-XX-Product-Guide-Web.pdf.
4. Storage, E.E. *Electrical Energy Storage - IEC*. 2016; Available from: www.iec.ch/whitepaper/pdf/iecWP-energystorage.
5. Sun, Y.G., Rogers, J. A., *Inorganic semiconductors for flexible electronics.* Advanced Materials, 2007. **19**(15): p. 1897-1916.
6. Pushparaj, V.L., Shaijumon, M. Manikoth, Kumar, Ashavani, Murugesan, Saravanababu, Ci, Lijie, Vajtai, Robert, Linhardt, Robert J., Nalamasu, Omkaram, Ajayan, Pulickel M., *Flexible energy storage devices based on nanocomposite paper.* Proceedings of the National Academy of Sciences of the United States of America, 2007. **104**(34): p. 13574-13577.
7. Jain, K., Klosner, M., Zemel, M., Raghunandan, S., *Flexible electronics and displays: High-resolution, roll-to-roll, projection lithography and photoablation processing technologies for high-throughput production.* Proceedings of the Ieee, 2005. **93**(8): p. 1500-1510.
8. Tehrani, Z., Korochkina, T., Govindarajan, S., Thomas, D. J., O'Mahony, J., Kettle, J., Claypole, T. C., Gethin, D. T., *Ultra-thin flexible screen printed rechargeable polymer battery for wearable electronic applications.* Organic Electronics, 2015. **26**: p. 386-394.
9. Kovalska, E., Kocabas, C., *Organic electrolytes for graphene-based supercapacitor: Liquid, gel or solid.* Materials Today Communications, 2016. **7**: p. 155-160.
10. Back, J., Tedesco,L., Fredi Molz,R. and Nara, E.,, *An embedded system approach for energy monitoring and analysis in industrial processes.* Energy, 2016. **115**(15 November): p. 811-819.
11. Beguin, F., Presser, V., Balducci, A., Frackowiak, E., *Carbons and Electrolytes for Advanced Supercapacitors.* Advanced Materials, 2014. **26**(14): p. 2219-2251.
12. Hauge, H.H., Presser, V., Burheim, O., *In-situ and ex-situ measurements of thermal conductivity of supercapacitors.* Energy, 2014. **78**: p. 373-383.
13. Simon, P., Gogotsi, Yury, *Materials for electrochemical capacitors.* Nature Materials, 2008. **7**(11): p. 845-854.
14. Miller, J.R., Simon, Patrice, *Materials science - Electrochemical capacitors for energy management.* Science, 2008. **321**(5889): p. 651-652.
15. Meng, C.Z.L., C. H.; Chen, L. Z.; Hu, C. H.; Fan, S. S. ,, *A Review of Flexible and Weaveable Fiber-Like Supercapacitors.* Nano Lett., 2010: p. 4025-4031.
16. Hu, L., Pasta, Mauro, La Mantia, Fabio, Cui, LiFeng, Jeong, Sangmoo, Deshazer, Heather Dawn, Choi, Jang Wook, Han, Seung Min, Cui, Yi, *Stretchable, Porous, and Conductive Energy Textiles.* Nano Letters, 2010. **10**(2): p. 708-714.

17. Chen, H., Wei, Bingqing, Ma, Dongsheng, *Energy Storage and Management System With Carbon Nanotube Supercapacitor and Multidirectional Power Delivery Capability for Autonomous Wireless Sensor Nodes.* Ieee Transactions on Power Electronics, 2010. **25**(12): p. 2897-2909.
18. Arico, A.S., Bruce, P., Scrosati, B., Tarascon, J. M., Van Schalkwijk, W., *Nanostructured materials for advanced energy conversion and storage devices.* Nature Materials, 2005. **4**(5): p. 366-377.
19. Kang, Y.J., Chung, H., Han, C. H., Kim, W., *All-solid-state flexible supercapacitors based on papers coated with carbon nanotubes and ionic-liquid-based gel electrolytes (vol 23, 065401, 2012).* Nanotechnology, 2012. **23**(28).
20. Choi, B.G., Hong, Jinkee, Hong, Won Hi, Hammond, Paula T., Park, HoSeok, *Facilitated Ion Transport in All-Solid-State Flexible Supercapacitors.* Acs Nano, 2011. **5**(9): p. 7205-7213.
21. Lota, G., Fic, K., Frackowiak, E., *Carbon nanotubes and their composites in electrochemical applications.* Energy & Environmental Science, 2011. **4**(5): p. 1592-1605.
22. Kim, B., Chung, Haegeun, Kim, Woong, *Supergrowth of Aligned Carbon Nanotubes Directly on Carbon Papers and Their Properties as Supercapacitors.* Journal of Physical Chemistry C, 2010. **114**(35): p. 15223-15227.
23. Baughman, R.H., Zakhidov, A. A., de Heer, W. A., *Carbon nanotubes - the route toward applications.* Science, 2002. **297**(5582): p. 787-792.
24. Hu, L., Choi, Jang Wook, Yang, Yuan, Jeong, Sangmoo, La Mantia, Fabio, Cui, Li-Feng, Cui, Yi, *Highly conductive paper for energy-storage devices.* Proceedings of the National Academy of Sciences of the United States of America, 2009. **106**(51): p. 21490-21494.
25. Chen, P., Chen, Haitian, Qiu, Jing, Zhou, Chongwu, *Inkjet Printing of Single-Walled Carbon Nanotube/RuO2 Nanowire Supercapacitors on Cloth Fabrics and Flexible Substrates.* Nano Research, 2010. **3**(8): p. 594-603.
26. Kaempgen, M., Chan, Candace K., Ma, J., Cui, Yi, Gruner, George, *Printable Thin Film Supercapacitors Using Single-Walled Carbon Nanotubes.* Nano Letters, 2009. **9**(5): p. 1872-1876.
27. Izadi-Najafabadi, A., Yasuda, Satoshi, Kobashi, Kazufumi, Yamada, Takeo, Futaba, Don N., Hatori, Hiroaki, Yumura, Motoo, Iijima, Sumio, Hata, Kenji, *Extracting the Full Potential of Single-Walled Carbon Nanotubes as Durable Supercapacitor Electrodes Operable at 4 V with High Power and Energy Density.* Advanced Materials, 2010. **22**(35): p. E235-+.
28. Kim, T.Y., Lee, Hyun Wook, Stoller, Meryl, Dreyer, Daniel R., Bielawski, Christopher W., Ruoff, Rodney S., Suh, Kwang S., *High-Performance Supercapacitors Based on Poly(ionic liquid)-Modified Graphene Electrodes.* Acs Nano, 2011. **5**(1): p. 436-442.
29. Liu, C., Yu, Zhenning, Neff, David, Zhamu, Aruna, Jang, Bor Z., *Graphene-Based Supercapacitor with an Ultrahigh Energy Density.* Nano Letters, 2010. **10**(12): p. 4863-4868.
30. Martinez, A.W., Phillips, S. T., Whitesides, G. M., *Three-dimensional microfluidic devices fabricated in layered paper and tape.* Proceedings of the National Academy of Sciences of the United States of America, 2008. **105**(50): p. 19606-19611.
31. Eder, F., Klauk, H., Halik, M., Zschieschang, U., Schmid, G., Dehm, C., *Organic electronics on paper.* Applied Physics Letters, 2004. **84**(14): p. 2673-2675.

32. Andersson, P., Nilsson, D., Svensson, P. O., Chen, M. X., Malmstrom, A., Remonen, T., Kugler, T., Berggren, M., *Active matrix displays based on all-organic electrochemical smart pixels printed on paper.* Advanced Materials, 2002. **14**(20): p. 1460-+.
33. Klemm, D., Heublein, B., Fink, H. P., Bohn, A., *Cellulose: Fascinating biopolymer and sustainable raw material.* Angewandte Chemie-International Edition, 2005. **44**(22): p. 3358-3393.
34. Standard, B.B., *Fixed electric double layer capacitors for use in electronic equipment. Part I: Generic specification*, in B.B. Standard, Editor. 2006, BSI British Standard.
35. Lehtimaki, S., Tuukkanen, Sampo, Porhonen, Juho, Moilanen, Pasi, Virtanen, Jorma, Honkanen, Mari, Lupo, Donald, *Low-cost, solution processable carbon nanotube supercapacitors and their characterization.* Applied Physics a-Materials Science & Processing, 2014. **117**(3): p. 1329-1334.
36. Keskinen, J., Sivonen, Eino, Jussila, Salme, Bergelin, Mikael, Johansson, Max, Vaari, Anu, Smolander, Maria, *Printed supercapacitors on paperboard substrate.* Electrochimica Acta, 2012. **85**: p. 302-306.
37. Lehtimaki, S., Li, Miao, Salomaa, Jarno, Porhonen, Juho, Kalanti, Antti, Tuukkanen, Sampo, Heljo, Petri, Halonen, Kari, Lupo, Donald, *Performance of printable supercapacitors in an RF energy harvesting circuit.* International Journal of Electrical Power & Energy Systems, 2014. **58**: p. 42-46.
38. Francois Beguin, E.F., *Supercapacitors: Materials, Systems and Applications*, T. Engineering, Editor. 2013.
39. Barcia, O.E., D'Elia, E., Frateur, I., Mattos, O. R., Pebere, N., Tribollet, B., *Application of the impedance model of de Levie for the characterization of porous electrodes.* Electrochimica Acta, 2002. **47**(13-14): p. 2109-2116.
35. Zhang X, Wang Y, Yang D, Chen Z. An on-line estimation of battery pack parameters and state-of-charge using dual filters based on pack model. Energy, Volume 115, Part 1, 15 November 2016, Pages 219-229
36. Farmann A, Waag W, Sauer D.U. Application-specific electrical characterization of high power batteries with lithium titanate anodes for electric vehicles. Energy, Volume 112, 1 October 2016, Pages 294-306
37. Rajanna, S. Saini R.P. Development of optimal integrated renewable energy model with battery storage for a remote Indian area. Energy, Volume 111, 15 September 2016, Pages 803-817